

PCCP

Accepted Manuscript



This is an *Accepted Manuscript*, which has been through the Royal Society of Chemistry peer review process and has been accepted for publication.

Accepted Manuscripts are published online shortly after acceptance, before technical editing, formatting and proof reading. Using this free service, authors can make their results available to the community, in citable form, before we publish the edited article. We will replace this *Accepted Manuscript* with the edited and formatted *Advance Article* as soon as it is available.

You can find more information about *Accepted Manuscripts* in the [Information for Authors](#).

Please note that technical editing may introduce minor changes to the text and/or graphics, which may alter content. The journal's standard [Terms & Conditions](#) and the [Ethical guidelines](#) still apply. In no event shall the Royal Society of Chemistry be held responsible for any errors or omissions in this *Accepted Manuscript* or any consequences arising from the use of any information it contains.



PCCP

PAPER

A Weight Averaged Approach for Predicting Amide Vibrational Bands of a Sphingomyelin Bilayer

Received 00th January 20xx,
Accepted 00th January 20xx

Kiyoshi Yagi,^{a,b} Pai-chi Li,^a Koichiro Shirota,^c Toshihide Kobayashi,^{c,d} and Yuji Sugita^{a,b,e,f,t}

DOI: 10.1039/x0xx00000x

www.rsc.org/

Infrared (IR) and Raman spectra of a sphingomyelin (SM) bilayer are calculated for the amide I, II, and A modes and the double bonded CC stretching mode by a weight averaged approach based on the all-atom molecular dynamics (MD) simulation and the vibrational structure calculation. Representative structures and statistical weights of SM clusters connected by the hydrogen bonds (HB) are observed in MD trajectories. After constructing smaller fragments from the SM clusters, the vibrational spectrum of the target modes is calculated by the normal mode analysis with correction for anharmonicity using the density functional theory. The final IR and Raman spectra of a SM bilayer are obtained as the weight averages over all SM clusters. The calculated Raman spectrum is in excellent agreement with the recent measurement, providing a clear assignment of the peak in question observed at 1643 cm⁻¹ to the amide I modes of a SM bilayer. The analysis of IR spectrum has also revealed that the amide bands are sensitive to the water content inside the membrane, since their band position is strongly modulated by the HB between SM and water molecules. The present study suggests that the amide I band serves as a marker to identify the formation of SM clusters and opens a new way to detect lipid rafts in the biological membrane.

1 Introduction

Sphingomyelin (SM) is one of the key constituents of a lipid raft,^{1,2} a segregated domain in the cell membrane, where SMs, glycosphingolipids, cholesterol, and specific proteins are selectively assembled. Lipid rafts are considered as platforms for various biological functions in the cell. Although the concept of lipid rafts has lasted for decades, there is still intense debate on the structural and dynamical features of lipid rafts.³ To resolve this issue, it is of fundamental importance to measure an aggregation and dynamics of SM in the membrane. Unlike glycerol-based lipids, SM can be either a hydrogen bond (HB) donor or acceptor (see Figure 1), thus can form clusters (dimer, trimer, and so on) in a bilayer. The dynamics of SM clusters has been extensively investigated using all-atom molecular dynamics (MD) simulations.⁴⁻⁶

Recently, Venable et al.⁶ have shown that the intermolecular HBs between NH ... OC and NH ... OH live long in a SM bilayer with decay times of 51 and 31 ns, respectively.

In this study, we focus on SM clusters in a lipid bilayer, computing the vibrational structures and comparing them with experimental measurements. Vibrational spectroscopy has been extensively used to provide the atomically detailed views of lipid bilayers.⁷ Experimental studies⁸⁻¹² based on the non-linear spectroscopy have successfully characterized the structural motifs of interfacial water in the vicinity of hydrophilic head groups. Nojima and Iwata^{13,14} have measured the viscosity inside lipid bilayers by probing the vibrational states of trans-stilbene embedded in the bilayers. Despite the abundant spectroscopic reports on lipids, those on SM have remained rather few.¹⁵⁻¹⁷ Recently, two of the authors (KS and TK) have found a prominent band at 1643 cm⁻¹ by the Raman spectroscopy on SM bilayers.¹⁸ Interestingly, it is also found that the band, clearly retained in a mixture of SM and dioleoyl-phosphatidylcholine (DOPC), is drastically reduced in a mixture of SM and dipalmitoyl-phosphatidylcholine (DPPC). Since SM is miscible with DPPC but not with DOPC,¹⁹⁻²¹ the observation suggests that the band serves as a marker of SM clusters and, potentially, that of lipid rafts. The character of the band has been deemed to be the amide I vibration of SM. In the previous studies, there were conflicts on the assignment.^{16,17} Levin et al.¹⁶ originally assigned a weak band in this region to the amide I mode. However, Lamba et al.¹⁷ later claimed that the band was the bending mode of water since the Raman activity was too weak. Theoretical analyses are thus needed to characterize each band clearly and to reveal the vibrational

^a RIKEN Theoretical Molecular Science Laboratory, 2-1 Hirosawa, Wako, Saitama 351-0198, Japan.

^b RIKEN ITHES, 2-1 Hirosawa, Wako, Saitama 351-0198, Japan.

^c RIKEN Lipid Biology Laboratory, 2-1 Hirosawa, Wako, Saitama 351-0198, Japan.

^d INSERM, Villeurbanne, France.

^e RIKEN Advanced Institute for Computational Science, 7-1-26 Minatojima-Minamimachi, Chuo-ku, Kobe, Hyogo 650-0047, Japan.

^f RIKEN Quantitative Biology Center, 1-6-5 Minatojima-Minamimachi, Chuo-ku, Kobe, Hyogo 650-0047, Japan.

^t E-mail: sugita@riken.jp; Fax: +81-48-467-4532; Tel: +81-48-462-1407.

Electronic Supplementary Information (ESI) available: Infrared intensity (Table S1) and Raman activity (Table S2) calculated for the fragment molecules in Fig. 5; IR and Raman spectrum calculated using two different definitions of HB (Figure S1); IR and Raman spectrum obtained with different length of time average (Figure S2); the order parameter ($|S_{CD}|$) with respect to carbon number of the tail groups of SM (Figure S3); the geometry of the fragment molecules in Fig. 5 obtained by DFT (Figure S4); See DOI: 10.1039/x0xx00000x

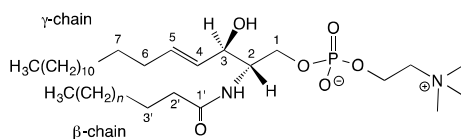


Fig. 1 The chemical structure of *N*-acyl sphingomyelin (SM). The sphingosine backbone (γ -chain) has double bonded carbons at the 4th and 5th position, whereas the β -chain is bonded to the backbone by an amide bond. The amide and hydroxyl groups serve as both HB donors and acceptors. The present study uses SMs with a chain length of $n = 12$, i.e., *N*-palmitoyl SM.

structure of SM bilayers.

There are three major issues for computing the vibrational spectrum of biological systems or molecules in the condensed phase with reliable accuracy. 1) In contrast to an isolated molecule in the gas phase, which is represented by only one or a few structures, molecules in the condensed phase interact and exchange the energy with the environment, thereby sample many transient structures that modulate the vibrational states. 2) Most vibrational modes of interest are fast, high-frequency modes that behave quantum mechanically. For example, the zero-point energy (500 - 2000 cm^{-1}) by far exceeds the thermal energy ($\sim 200 \text{ cm}^{-1}$ at the room temperature), so that the phase space volume of such vibration is much smaller in classical mechanics than in quantum mechanics. 3) The accuracy of the spectrum, i.e., the frequency and the transition intensity, is strongly dependent on the quality of the electronic structure theory to compute the electronic energy and properties such as dipole moments. A rigorous treatment that covers all these issues calls for a full quantum dynamics simulation based on accurate electronic structure theories propagated for sufficiently long time to make an ensemble average. However, the cost of such calculation is beyond the reach of current computational resources.

One of the viable approaches is the mixed quantum-classical (Q/C) method,²²⁻²⁶ where the vibrational modes of interest are treated by quantum mechanics, while the other bath modes by classical mechanics. Recently, Skinner and coworkers²⁷⁻²⁹ have computed the vibrational spectrum of water in a hydrated lipid-bilayer system treating the OH/OD stretching vibration in quantum mechanics and the other motions classically. The key technique that has made a long-time sampling of the system feasible is the use of a mapping function,³⁰⁻³² which gives the vibrational frequencies and transition properties from the electrostatic field at a reference position (i.e., oxygen and hydrogen atoms of the water) alleviating the intensive quantum equations for both electrons and vibrations. The amide I band of peptides and proteins has been extensively studied by many groups³³⁻³⁸ in a similar approach combining the vibrational exciton model with a mapping function that represent the frequency as well as the coupling interaction between the nearest neighbor amides.³⁹ However, the mapping function is not available for every vibrational mode. Although the amide I mode of polypeptides and the OH stretching mode of water have been extensively tested, targeting other vibrational modes requires a development and validation of the mapping function. Tavan

and coworkers⁴⁰⁻⁴⁴ have calculated the vibrational spectrum by the instantaneous normal mode analysis (INMA), in which the vibrational structure of the molecule of interest is calculated based on an electronic structure calculation combining the density functional theory with the molecular mechanics environment (DFT/MM) at every snapshot of the classical MD simulation and averaged along the trajectory. The explicit treatment of electrons and vibrations has enabled a wide variety of applications ranging from solute-solvent systems^{40,41} to chromophores in a protein.⁴²⁻⁴⁴ One of the major drawbacks is the cost of DFT calculation, which limits the length of sampling time. Furthermore, the method assumes a spatial decomposition of the system into DFT and MM region, and thus is not readily applicable to the condensed phase system, for instance, lipid bilayers.

In the present study, we propose a new approach combining the all-atom MD simulation and the vibrational structure calculation to predict the infrared (IR) and Raman bands of amide modes of SM clusters in the lipid bilayer. First, the all-atom MD simulation is carried out for a SM bilayer, and the resulting trajectory is analyzed to detect the SM clusters and to obtain their statistical weights. Then, the harmonic vibrational analysis is performed for each SM cluster based on DFT. The SM cluster is approximated to molecular fragments in the vicinity of amide groups and their HB partners (i.e., OH groups and waters) with neglect of the head and tail groups of SM to reduce the cost of the DFT calculation. In order to account for the anharmonicity, the harmonic frequency is scaled by a mode-specific factor, which is derived from anharmonic vibrational structure calculations carried out for a single SM molecule. Finally, the vibrational spectrum is calculated as the weight average of the spectrum over all SM clusters. We emphasize that the key idea of the present approach is the clustering and the weight average that keeps the number of DFT calculations small while accounting for the dynamical fluctuation of a SM bilayer. We show that the computational procedure in this study provides an accurate spectrum comparable to the experiment and that the Raman band in question is unambiguously assigned to the amide I mode of SM clusters in a bilayer.

The paper is organized as follows. Section 2 presents the details on the MD, DFT, and the vibrational structure calculations to compute the IR and Raman spectrum. The results of these calculations are discussed in Section 3. The concluding remarks are given in Section 4.

2 Method

The all-atom MD simulation was performed using the NAMD simulation package⁴⁵ with the CHARMM c36⁶ and TIP3P⁴⁶ for SM and water, respectively. A small membrane patch, which contained 32 SMs and 1280 water molecules, was built by CHARMM-GUI.⁴⁷ The head group of SM was placed in a hexagonal lattice, where the area per lipid was set to 46 \AA^2 and the distance between the top and bottom layers was set to 52 \AA . The small patch was energy-minimized and equilibrated for 10 ns by the MD simulation. Then, four copies of the small

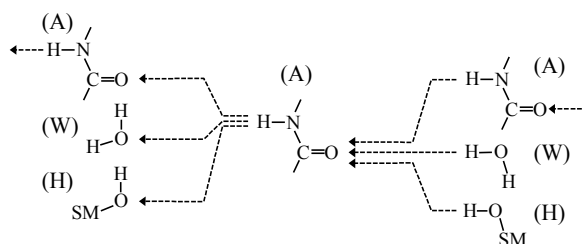


Fig. 2 The HB connectivity of the amide group, hydroxyl group, and water considered in this work.

patch were combined to construct a 128-lipid system, which was subjected to an equilibration run for 10 ns and a production run for 150 ns. The bond length involving hydrogen atoms was restrained by the SHAKE method⁴⁸ and the time step for integration was set to 2 fs. The period boundary condition was used in all direction. The electrostatic interaction was calculated using the smooth Particle-Mesh Ewald method.^{49,50} The non-bonding interaction was reduced to zero between 10 and 12 Å employing a switching function. The neighbor list was updated every 20 fs. Langevin thermostat was used to control the target temperatures with the coupling time set to 1 ps⁻¹. Two different MD simulations were carried out at 23 and 50 °C, respectively. The semi-isotropic pressure was kept at 1 bar by the Nosé-Hoover Langevin piston method⁵¹⁻⁵³ with the oscillation period time and the damping time set to 50 fs and 25 fs, respectively. The trajectory was saved every 10 ps. The 10,000 frames in total were used for the further analysis. All the illustrations were prepared using VMD.⁵⁴

The main focus of the present study is to elucidate the effect of HB on the amide vibrations in SM. To this end, let us denote the amide group, the hydroxyl group, and the water molecule as A, H, and W, respectively (see Figure 2). A SM bilayer is divided into different types of SM clusters using these notations. The actual procedure is based on the HB network in the vicinity of the amide group as follows:

1. Search for an amide group, in which the NH bond is NOT hydrogen bonded with another amide group. If the NH bond is free from HB, set the type of the current cluster to 'A'. Otherwise, if the NH bond is hydrogen bonded to the hydroxyl group or water, set the type to 'HA' or 'WA', respectively.
2. Search for a HB donor to the CO bond of the amide group, and add the name of the donor (A, H, and/or W) to the right of the type.
3. If the CO bond accepts another amide group, increment the amide group to the newly found one and return to step 2. Otherwise, the type of the current cluster is set.
4. Return to step 1 until all the amide groups are assigned to the SM clusters found.

Note that the CO bond may accept two HB donors. Thus, two groups may follow after the current A in step 2. For example, when the CO bond accepts W and H, the type is set to be AHW. If the CO bond accepts two amide groups, the cluster type is bifurcated using parentheses as A(A··)A··, though such a case was not encountered in this work. The HB between X-H ... Y (X

and Y being either oxygen or nitrogen atoms) is defined in terms of the X-Y distance (r_{XY}) and the angle between H-X and X-Y (θ_{HXY}) as,

$$r_{XY} < 3.5 \text{ \AA} \text{ and } \theta_{HXY} < 30.0^\circ. \quad (1)$$

Eq. (1) is a definition commonly used for HB analyses in MD programs. We have tested another definition ($r_{XY} < 3.2 \text{ \AA}$ and $\theta_{HXY} < 150.0^\circ$) and confirmed that the change is small in the resulting spectrum (shown in Fig. S1 of the supporting information (SI)).

In the above algorithm, the amide group is uniquely assigned to each SM cluster. Therefore, the statistical weight of a cluster type T is given as,

$$c_T = \frac{N_T N_A^T}{N_A}, \quad (2)$$

where N_T , N_A^T , and N_A are the number of cluster type T found in the trajectory, the number of the amide groups in cluster type T , and the total number of amide groups considered (i.e., 128), respectively. Note that c_T is normalized as,

$$\sum_T c_T = 1. \quad (3)$$

The vibrational spectrum was then computed for each cluster by the DFT method using Gaussian09.⁵⁵ The water molecule was used as is, while the SM molecules were reduced to a fragment in the vicinity of the amide or hydroxyl group (see Section 3.2. for details). A representative structure was searched for each cluster by the k -means clustering method⁵⁶ as implemented in the MMTSB Toolset.⁵⁷ The clustering was carried out using the root-mean square deviation (RMSD) of the heavy atoms as a measure of the distance between the clusters. The clustering radius was set to 1.5 Å. The DFT calculation was carried out for the structure using the B3LYP exchange-correlation functionals^{58,59} with 6-31G(d,p) and 6-31++G(d,p) basis sets.⁶⁰⁻⁶² The diffuse functions were employed only for the amide atoms (O, C, N, H) and those involved in the hydrogen bonds (water and the hydroxyl group). The combined basis set is denoted 6-31(++)G(d,p) in the following. The geometry of the cluster (SM fragment and water) was optimized fixing the relative orientation of SMs in the cluster, i.e., the dihedral angle formed by C1 and C2 atoms in Fig. 1 of two SMs. The vibrational analysis was carried out at the optimized geometry to obtain the harmonic frequency, IR intensity, and Raman activity. Since the normal modes were a mixture of several types of motion, the amide I, II, and A modes were identified by monitoring an overlap between the normal displacement vector and the CO stretching, NH bending, and NH stretching motion, respectively, and adopting when the overlap was larger than 0.4. In this way, the number of amide modes coincided with the number of amide groups (i.e., SM molecules) in the cluster in almost all types of cluster. An exception was clusters that had a motif of 'AWW', which often had more than one amide I modes identified due to a strong resonance between the CO stretching and the water bending motions. In such case, the resonant modes were all adopted as the amide I modes.

The vibrational spectrum is calculated by the following equation,

$$R(\nu) = \left\langle \sum_T \frac{c_T}{N_A^T} \sum_{\nu}^{\text{mode}} R_{\nu}^T \Gamma(\nu - \nu_{\nu}^T) \right\rangle, \quad (4)$$

where ν , ν_{ν}^T , and R_{ν}^T are an index of the amide vibrational mode, the transition frequency, and the intensity of the mode ν of the cluster type T , respectively, and $\Gamma(\nu - \nu_{\nu}^T)$ is a line shape function centered around ν_{ν}^T ,

$$\Gamma(\nu - \nu_{\nu}^T) = \frac{2}{\pi} \left[\frac{\gamma}{4(\nu - \nu_{\nu}^T)^2 + \gamma^2} \right], \quad (5)$$

with $\gamma = 15 \text{ cm}^{-1}$. Note in Eq. (4) that the weight is divided by N_A^T , because N_A^T amide bands are already summed in the spectrum of the cluster type T . ν_{ν}^T is obtained by correcting the harmonic frequencies of SM clusters (ω_{ν}^T) as,

$$\nu_{\nu}^T = f_{\nu} \times (\omega_{\nu}^T + \delta\omega_{\nu}), \quad (6)$$

where f_{ν} accounts for the anharmonicity and $\delta\omega_{\nu}$ is the correction for the fragment size and the basis set error. f_{ν} is obtained from anharmonic vibrational calculations at the vibrational MP2⁶³ (VMP2) level based on a quartic force field⁶⁴ for a single SM fragment using SINDO program.⁶⁵ Note that the same correction was applied to the mode ν irrespective to the cluster type. The assumption may be critical since the formation of HB may enhance the anharmonicity that alters the value of f_{ν} . We discuss this point in Section 3.3. As for the transition intensity, R_{ν}^T , the IR intensity and the Raman activity calculated at the B3LYP/6-31(++)G(d,p) level were used as is. The time average was performed by dividing the 100-ns trajectory in 10-ns bits (thus 10 pieces). The clustering as well as DFT calculations were performed for each bit and the resulting 10 spectra were averaged to obtain the final spectrum. The average was well converged with respect to the time length (shown in Fig. S2). In each bit, about 20 cluster types were found, so that the total number of clusters amounted to 200. The DFT calculations were run in parallel for each cluster using the supercomputer.

We note that the present scheme, Eq. (4), is based on an assumption that the molecular (amide) vibration can be taken to be in the inhomogeneous limit [Eq. (5)]. It may be reasonable regarding the lipid motion, because the timescales of the vibrational motion ($< 1 \text{ ps}$) and the lipid motion (tens of ns) are substantially different. However, it may not be the case for other motion in an intermediate timescale, such as intermolecular motion, HB rearrangement of water, and so on. The neglect of a dynamical coupling between the amide vibration and such motion may cause an error in the line shape, which will be assessed in Section 3.

The vibrational spectrum of the double bonded CC stretching mode was calculated in a similar, but much simpler way, since the CC double bond does not participate in the HB representative structure was searched by the k -means clustering method. This procedure yielded 7 - 9 conformers in every 10 ns, which were different in the dihedral angles about the CC single bonds. The subsequent DFT calculations were network. Fragment molecules in the vicinity of the CC group (see Section 3.2.) were collected from the trajectory and the performed at the B3LYP/6-31(++)G(d,p) level with the diffuse

functions added only to the double bonded carbon atoms. We have found that the Raman activity of the CC stretching mode calculated by B3LYP largely deviates from the MP2 value (85 versus $32 \text{ \AA}^4 \text{ amu}$, respectively). Since MP2 is more reliable for computing the polarizability needed to obtain the Raman activity,⁶⁶ the Raman activity obtained from B3LYP was scaled by $32/85$ to account for the error. Using the CC stretching frequency and intensity thus obtained, the final spectrum has been calculated as the weight average over the conformation and time.

3 Results

3.1 Molecular Dynamics Simulation

Two all-atom MD simulations have been performed at $50 \text{ }^{\circ}\text{C}$ and $23 \text{ }^{\circ}\text{C}$, respectively. The former temperature is the same as that in the previous MD work⁶ and the latter is the temperature in which the Raman spectrum was measured experimentally.¹⁸ The structural parameters of the bilayer are summarized in Table 1. The averaged phosphate-phosphate separation (d_{pp}) and the area per lipid (A_L) at $50 \text{ }^{\circ}\text{C}$ agree well with those reported in the previous MD study⁶ within the statistical errors. The averaged order parameters are also in excellent agreement with the previous MD⁶ and NMR.⁶⁷

SM bilayers undergo a phase transition from the liquid crystal (LC) to gel phase at $38 \text{ }^{\circ}\text{C}$, so that the simulation at $23 \text{ }^{\circ}\text{C}$ should yield the bilayer structure in the gel phase. The snapshot of the SM bilayer is shown in Figure 3. It is visually

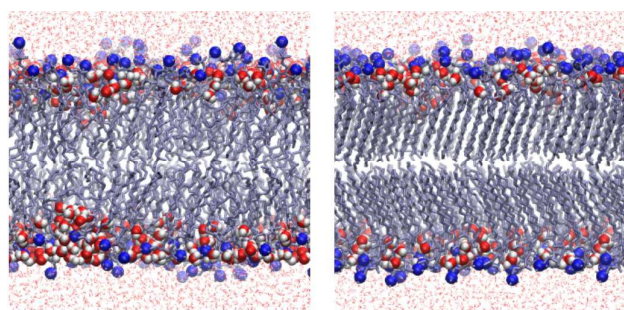


Fig. 3 The final structure of a SM bilayer obtained from the simulations at $50 \text{ }^{\circ}\text{C}$ (left) and $23 \text{ }^{\circ}\text{C}$ (right). Nitrogen atoms of the choline group are drawn in blue. The highlighted waters are those inside the membrane, i.e., beyond the average position of the choline nitrogens along the membrane normal.

Table 1. The phosphate-phosphate separation (d_{pp}), the area per lipid (A_L), and the averaged order parameter ($\langle S_{CD}^{\text{plat}} \rangle$ and $\langle S_{CD} \rangle$) obtained in this work compared with the previous MD and NMR.

	$T / \text{ }^{\circ}\text{C}$	$d_{pp} / \text{ \AA}$	$A_L / \text{ \AA}^2$	$\langle S_{CD}^{\text{plat}} \rangle^a$	$\langle S_{CD} \rangle^b$
This work	50	40.5 ± 0.5	55.8 ± 0.9	0.254	0.221
	23	43.5 ± 0.2	47.5 ± 0.2	0.285	0.284
MD ^c	50	40.7	55.4	0.257	-
NMR ^d	48	-	-	0.253	0.221

^a An average over a plateau region (C5 to C9) of the β -chain. ^b An average over C4 to C15 of the β -chain. ^c Reference ⁶. ^d Reference ⁶⁷.

Table 2. Averaged probabilities of hydrogen bond partners of NH, CO, and OH groups in SM bilayers obtained from MD simulations in the LC and gel phases.

Acceptor	NH		CO			OH					
	LC	Gel	Donor	LC	Gel	Acceptor	LC	Gel	Donor	LC	Gel
CO	0.23	0.36	water and NH ^a	0.07	0.17	PO ₄ ^b	0.89	0.92	NH	0.21	0.25
PO ₄	0.03	0.01	NH	0.17	0.19	water	0.01	0.00	water	0.52	0.37
OH	0.21	0.25	two waters ^a	0.26	0.12	none	0.11	0.08	none	0.27	0.38
water	0.37	0.24	one water	0.44	0.37						
none	0.17	0.15	none	0.07	0.16						

^a CO accepting two hydrogen bond donors. ^b Intramolecular hydrogen bonds. Others are all intermolecular ones.

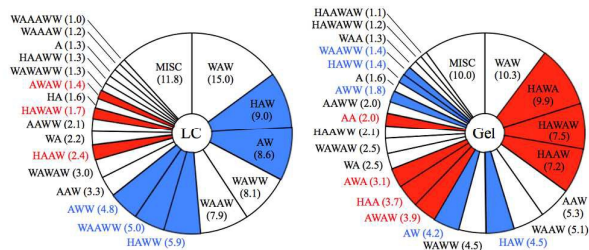


Fig. 4 The type and the statistical weight (in percentage) of hydrogen-bonded SM clusters obtained from the HB analysis on the 100-ns trajectory of a SM bilayer in the LC (left) and gel (right) phases. The cluster types that increase or decrease more than twice are colored in red or blue, respectively, upon the change from the LC phase to the gel phase.

confirmed that the tail groups are kept well ordered at 23 °C, while they are rather disordered at 50 °C. Accordingly, the averaged order parameter ($\langle |S_{CD}| \rangle$) in Table 1 is significantly increased at 23 °C. Note that the order parameters not only increase in magnitude but also exhibit a wide plateau ranging from C3 to C15 ($|S_{CD}|$ versus the carbon number is plotted in Fig. S3). Table 1 also shows that the bilayer has longer d_{pp} and smaller A_L at 23 °C than at 50 °C, which is a trend generally expected upon cooling. The effective volume per lipid ($d_{pp} \times A_L$) is reduced by 7 % upon the change from the LC to gel phase. These results indicate that the present MD simulations yield reliable models of a SM bilayer in the LC and gel phases. Hereafter, we refer to the results at the high and low temperature as those in the LC and gel phases, respectively.

The HB partners of NH, CO, and OH groups have been searched in the final 100-ns trajectory and their averaged probabilities are listed in Table 2. It is notable that the contribution of water is decreased for all groups upon going from the LC to gel phase. For example, the number of the NH groups donating to waters decreases from 0.37 to 0.24. This is because the membrane contains less number of waters in the gel phase than in the LC phase; see the amount of highlighted waters in Fig. 3. The number of waters inside the membrane is found to be 3.9 and 2.1 per lipid in the LC and gel phases, respectively. The decrease of waters induces a higher connectivity of the amide groups. The number of the NH groups donating to the CO increases from 0.23 to 0.36. Similarly, the CO groups accepting waters are replaced by those accepting the NH groups (and those without HB).

Therefore, the SM bilayer has longer chain of hydrogen-bonded amide groups in the gel phase: the chain length is extended from 1.54 to 1.76 on average.

The type and the statistical weight of SM clusters obtained from the HB analysis are shown in Figure 4. In both LC and gel phases, the most dominant cluster type is WAW. However, the major cluster types are found to be markedly different after WAW. HAW and AW, which are dominant in the LC phase, decrease by half in the gel phase. Instead, dimers of the amide group, i.e., HAWA, HAWAW, and HAAW, increase in the gel phase. In particular, the increase of HAWA is remarkable; the weight in the LC phase being 0.29 % increase by more than 30 times to 9.9 % in the gel phase. This result is consistent with the finding that waters in the membrane decrease in the gel phase. For example, the weight of WAW decreases from 15.0 to 10.3 %. Also, the CO groups accepting two waters (HAWW, WAAWW, AWW) prominently decrease in amount. These results reinforce that the SM bilayer has less amount of water and higher connectivity of the amide group in the gel phase than in the LC phase.

In Table 2, the OH group is found to be exclusively donating to the phosphate group both in the LC and gel phases. Note that the force-field parameters for SM have been refined in the previous work⁶ so that the OH group prefers an intramolecular HB with the phosphate group in accordance with the recent NMR measurement. Consequently, the cluster type, in which the OH group donates to the CO group (such as AH), is never encountered. As an acceptor, the weight of OH groups accepting waters decreases from 0.52 to 0.37 in the gel phase.

3.2. Quantum Chemistry Calculations

The computation of vibrational spectra requires an accurate electronic structure calculation, since the frequency, IR intensity, and Raman activity are sensitive to the variation of the electronic potential energy, dipole moment, and polarizability, respectively, as a function of nuclear coordinates. However, it is infeasible to apply the most accurate electron correlation theory to all the SM clusters found in Section 3.1. Therefore, the downsizing of SM clusters as well as judicious selection of the electronic structure theory is necessary. In this subsection, we assess the size of the fragment and the level of electronic structure calculations for computing the amide and CC stretching bands of SM.

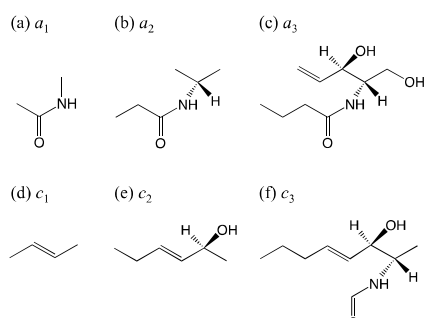


Fig. 5 Fragments of SM used to calculate the amide vibrations [(a)-(c)] and the double bonded CC stretching vibration [(d)-(f)]. n of a_n and c_n ($n = 1, 2, 3$) denotes the number of chemical groups extended, starting from the amide group and the CC moiety, respectively.

Table 3. Harmonic frequencies (in cm^{-1}) of the amide and CC stretching modes calculated for the fragment molecules in Fig. 5 using various electronic structure methods and basis sets.

frag.	method	basis	Amide ^a			CC str.
			I	II	A	
a_2/c_2	B3LYP	cc-pVDZ	1765	1535	3593	1750
a_2/c_2	B3LYP	aug-cc-pVDZ	1724	1534	3613	1739
a_2/c_2	B3LYP	(aug)-cc-pVDZ ^b	1725	1532	3616	1744
a_2/c_2	B3LYP	(aug)-cc-pVTZ ^b	1730	1531	3620	1735
a_2/c_2	B3LYP	(aug)-cc-pVQZ ^b	1732	1532	3618	1734
a_2/c_2	B3LYP	CBS	1733	1532	3618	1733
a_2/c_2	BLYP	(aug)-cc-pVDZ ^b	1645	1469	3495	1674
a_2/c_2	B3LYP	(aug)-cc-pVDZ ^b	1725	1532	3616	1744
a_2/c_2	LC-BLYP	(aug)-cc-pVDZ ^b	1816	1593	3688	1847
a_2/c_2	MP2	(aug)-cc-pVDZ ^b	1715	1540	3638	1728
a_1/c_1	B3LYP	(aug)-cc-pVDZ ^b	1751	1556	3662	1743
a_2/c_2	B3LYP	(aug)-cc-pVDZ ^b	1725	1532	3616	1744
a_3/c_3	B3LYP	(aug)-cc-pVDZ ^b	1731	1537	3620	1740
a_3/c_3^c	B3LYP	CBS	1739	1537	3622	1729

^a I, II, and A correspond to the CO stretching, NH bending, and NH stretching modes, respectively. ^b Diffuse functions are added only to the amide atoms (N, H, C, and O) or to the double bonded carbons. ^c Frequencies estimated by Eq. (8).

The harmonic frequencies of the amide and CC stretching modes have been calculated for fragments of SM shown in Figure 5 by several DFT methods and the MP2 method⁶⁸ using a series of Dunning's basis sets.⁶⁹ The results are listed in Table 3 and the optimized geometry is shown in Fig. S4. A large difference is found between the cc-pVDZ and aug-cc-pVDZ results based on B3LYP for the amide I and A modes (41 and 20 cm^{-1} , respectively), indicating that the diffuse functions are indispensable. On the other hand, the results of (aug)-cc-pVDZ basis sets, in which the diffuse functions are added only to the amide (N, H, C, and O) and the double bonded carbon atoms, are found to be in excellent agreement with the aug-cc-pVDZ results with the largest deviation being as small as 5 cm^{-1} . Furthermore, the (aug)-cc-pVXZ results with X = D, T, and Q are found to be smoothly converging, suggesting that the high-angular momentum basis sets play a minor role. The series of frequencies is well represented by the three-point

Table 4. Harmonic and anharmonic frequencies (ω_v and ν_v , respectively, in cm^{-1}) of the amide and CC stretching modes of a_2 and c_2 , respectively, calculated at the B3LYP/6-31(++)G(d,p) level of theory and the parameters in Eq. (6).

	Amide ^a			CC str.
	I	II	A	
ω_v	1742	1541	3629	1745
ν_v^b	1709	1485	3472	1703
f_v	0.981	0.964	0.957	0.976
$\delta\omega_v$	-3	-4	-7	-16
ν_v^{SM}	1706	1482	3464	1687

^a I, II, and A correspond to the CO stretching, NH bending, and NH stretching modes, respectively. ^b Calculated by VMP2 method.

extrapolation formula suggested by Peterson et al.,⁷⁰

$$\omega(l) = \omega(\text{CBS}) + A \exp[-(l-1)] + B \exp[-(l-1)^2] \quad (7)$$

where $l = 2, 3$, and 4 correspond to the cardinal number of the basis sets, X = D, T, and Q, respectively. The frequency at the complete basis set (CBS) limit obtained from Eq. (7) is listed in Table 3.

Table 3 also compares the performance of pure DFT (BLYP), hybrid DFT (B3LYP), and long-range corrected DFT⁷¹ (LC-BLYP) with that of MP2. It is found that both BLYP and LC-BLYP frequencies severely deviate from the MP2 frequencies with the mean absolute deviation (MAD) of 85 and 80 cm^{-1} , respectively. Note that the sign of deviation is opposite between BLYP and LC-BLYP. B3LYP results lie in the middle of them yielding the frequency in good agreement with MP2 with MAD of 14 cm^{-1} .

Finally, the results of a_n ($n = 1, 2$, and 3) show that the variation is reduced from 24 cm^{-1} to 5 cm^{-1} on average upon going from $n = 1 \rightarrow 2$ and $n = 2 \rightarrow 3$. The CC stretching mode is found to be relatively insensitive to the size with small variation with respect to n . These data provide an estimate of the harmonic frequency of a_3/c_3 at the CBS limit as,

$$\omega_v(x_3@\text{CBS}) = \omega_v(x_2@\text{adz}) + \omega_v(x_2@\text{CBS}) - \omega_v(x_2@\text{adz}) \quad (8)$$

where x_n is either a_n or c_n , and adz stands for (aug)-cc-pVDZ. The frequency obtained from this formula is listed in the last row of Table 3.

The results in Table 3 suggest that the use of the a_2/c_2 fragment and the B3LYP/6-31(++)G(d,p) level of theory is reasonable for calculating the spectrum of SM. Note that we have employed 6-31(++)G(d,p) in place of (aug)-cc-pVDZ to reduce the computational cost. Using this level, the anharmonic frequencies have been calculated by the VMP2 method. Listed in Table 4 are the resulting harmonic and anharmonic frequencies (ω_v and ν_v , respectively) together with the parameters in Eq. (6) obtained by,

$$f_v = \nu_v / \omega_v, \quad (9)$$

$$\delta\omega_v = \omega_v(x_3@\text{CBS}) - \omega_v. \quad (10)$$

Table 4 clearly shows that the effect of anharmonicity is sizable, affecting the frequency of amide A mode as much as 157 cm^{-1} and that of the other modes by 30 - 50 cm^{-1} . Although a constant factor (f) is often used for every mode to account for the anharmonicity by $\nu = f\omega$, f_v in Table 4 shows that the scaling in fact depends on the mode varying in the range of

0.96 - 0.98. Since the difference in f_v by 0.01 amounts to tens of wavenumber in the scaled frequency, the result demonstrates the importance of mode-specific correction for quantitative purposes. Interestingly, the anharmonic effect is larger for the modes related to the motion of hydrogen atoms (amide II and A modes) than those related to the motion of heavy atoms (amide I and CC stretching modes). $\delta\omega_v$ is found to be reasonably small for every mode attesting the accuracy of the electronic structure theory employed. The vibrational frequencies of a single SM molecule (ν_v^{SM}) obtained from Eq. (6) are listed in the last row of Table 4.

3.3. Theoretical Raman spectrum

The calculated Raman spectrum is shown in Figure 6 together with the observed one in a region where the CC stretching and amide I modes reside. The calculated Raman spectrum shows a prominent band around 1685 cm^{-1} , which originates from the CC stretching mode (shown in green). The amide I bands of the monomers (WAW, HAW, etc.) and dimers (WAAW, HAWA, etc.) are shown in blue and red, respectively. In the LC phase, the monomers constitute a prominent band at 1667 cm^{-1} . However, the band largely overlaps with the intense CC stretching band, and it appears only as a vague shoulder in the total spectrum. The dimer band is red-shifted and has less overlaps with the CC stretching band. Nevertheless, it does not

yield any peak in the total spectrum due to the fractional weight of the dimers. Consequently, the total spectrum obtained from the sum of these three components appears as a single band asymmetrically broadened in the low frequency side.

In contrast, the Raman spectrum in the gel phase, displayed in the middle panel of Fig. 6, exhibits a clear trace of the amide I band in the low frequency region. This is because the dimers increase in the gel phase due to the decrease of waters from the membrane as discussed in Section 3.1. The growth of the dimer band is noticeable in a wide region of 1640 - 1670 cm^{-1} , yielding a plateau-like shape in the total spectrum. The spectrum thus obtained is in excellent agreement with the experimental spectrum (the bottom panel of Fig. 6). Therefore, the character of the band at 1676 cm^{-1} and the plateau around 1655 cm^{-1} in the experimental spectrum is unambiguously assigned to the CC stretching mode and the amide I mode of the SM bilayer, respectively.

Nevertheless, it is notable that the calculated spectrum is somehow broader in the low frequency side compared to the experiment. The band around 1640 cm^{-1} seems to be too intense. One of the possible reasons may be the intrinsic accuracy of electronic and vibrational structure methods to calculate the band position and the Raman activity. The other drawback of the present method is the lack of dynamical coupling in computing the band shape. In general, an explicit account of the vibrational dynamics makes the line shape narrower (the so-called motional narrowing).

The Raman measurement has found that the shape of the amide I band is sensitive to the water content of the membrane, where a prominent second band grows at 1643 cm^{-1} in a dried condition.¹⁸ Although a simulation with fewer amount of waters is not attempted, the variation of the spectrum in the LC and gel phase suggests that the dried condition should induce an increase in the number and size of SM clusters that leads to a further growth of the amide I band. These results indicate that the water content strongly affects the HB network of the SM bilayer and the spectral shape of the amide I band. Thus, the water content of the sample may be one of the reasons that the amide I band has been clearly observed in our recent measurement in contrast to the earlier studies.

3.4. Theoretical IR spectrum

The IR spectrum of the SM bilayer has been reported in the previous works,^{17,72,73} which was measured in the heavy water to avoid an overlap of the water bending and the amide I bands. The spectra measured at 24 and 54 °C by Arsov and Quaroni⁷³ are displayed in Figure 7 (c). The band shape analyses have revealed that the high frequency component (~1650 cm^{-1}) increases relative to the low frequency one (~1630 cm^{-1}) upon the increase of temperature (i.e., the change of phase from gel to LC).

We calculated the IR spectrum of deuterated system by substituting the mass of hydrogen atoms of water and amide group to that of deuterium when constructing the mass

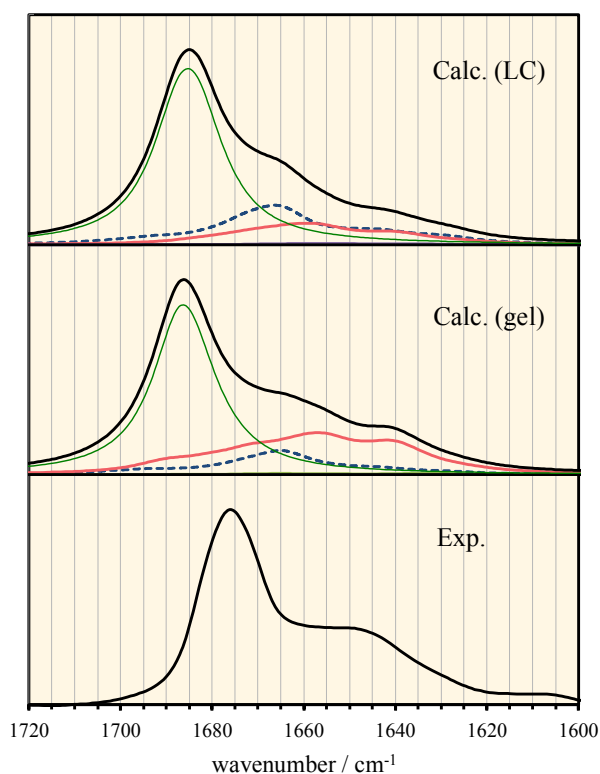


Fig. 6 (Top and middle) Calculated Raman spectrum of a SM bilayer in the LC and gel phases. The blue (broken) and red (solid thick) lines are the amide I bands of the monomers and dimers of the amide group, respectively. The green (solid thin) line is the CC stretching band. The black line is the total intensity. (Bottom) Raman spectrum measured for SM bilayers at 23 °C.

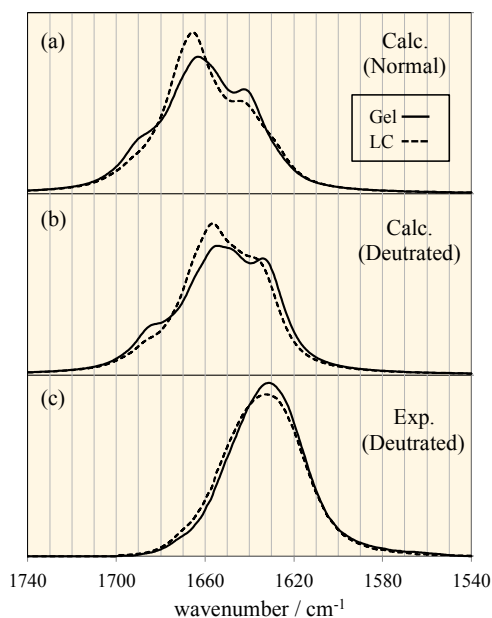


Fig. 7 IR spectrum in a region of amide I and CC stretching modes of a SM bilayer in the gel (bold line) and LC (broken line) phase. (a) Calculated IR spectrum of a SM bilayer with normal hydrogen. (b) The same as (a) but with deuterated water (D_2O) and amide group (ND). (c) The experimental spectrum taken from Ref. [73] measured in deuterated water at $24\text{ }^\circ\text{C}$ (bold line) and $54\text{ }^\circ\text{C}$ (broken line).

weighted Hessian matrix. Note that the weight of cluster types was kept the same in the average of the spectrum, and that the MD simulation is not repeated for the deuterated system. The spectra of the normal and deuterated systems are shown in Figure 7 (a) and (b), respectively. The effect of the deuterium substitution on the amide I band is non-negligible, shifting the band position lower by as much as 10 cm^{-1} . This is because the amide I mode is not purely the CO stretching motion, but slightly mixed with the NH bending motion. The increase in the associated mass causes the decrease of the vibrational frequency. The band position of the deuterated system compares reasonably well with the experimental one with an accuracy of $\sim 10\text{ cm}^{-1}$. The tendency upon the change of phase is somehow reproduced as well. However, the calculated spectrum gives a bumpy feature, which is absent in the experimental spectrum. An excessive intensity of some bands may be an artifact due to the neglect of dynamical coupling between the amide I mode and the environment.

Although the accuracy is found to be limited regarding the band shape, it is still interesting to decompose and analyse the amide bands to draw physical insight from the spectrum. The calculated IR spectrum in the gel phase is shown in Fig. 8 (a) together with the spectra decomposed in terms of the amide modes of monomers and dimers (in blue and red, respectively), and the CC stretching mode (in green). In contrast to the Raman spectrum, the CC stretching band found at 1687 cm^{-1} is much weaker in intensity than the amide I band, thereby contributing little to the total spectrum. As for the amide bands, it is notable that the dimer band is red-shifted for the amide I and A modes compared to that of monomers, while it is blue-shifted for the amide II mode. Also found in Fig. 8 (a) is

a fine structure in each amide band with several peaks. In order to understand the variation of the monomer and dimer spectrum and the origin of the peaks, we have further decomposed the amide bands in terms of major cluster types shown in Fig. 4. The resulting spectra are shown in Fig. 8 (b) and (c) for the monomers and dimers, respectively. In Fig. 8 (c) and hereafter, the amide group, to which the amide mode of dimers is assigned, is denoted with quotations as 'A'. For example, the amide I band of $H'A'WA$ is the CO stretching mode of the first amide group, where the CO bond accepts a water and a NH bond of the second amide group. For the sake of analyses, we have also calculated the HB interaction energy of the SM clusters, which is listed in Table 5.

In the amide I region, the shoulder band at 1689 cm^{-1} arises from the CO bond of $HAW'A'$, where the CO bond is free from HB but the NH bond donates to HA. Note that the peak position is red-shifted by 17 cm^{-1} compared to that of the isolated amide group at 1706 cm^{-1} (see Table 4) due to the HB of the NH bond. The main peak at 1663 cm^{-1} originates from the CO bond accepting one water; for example, WAW of monomers and $HA'A'W$ of dimers. The amide I bands of the CO bond accepting the amide group ($H'A'AW$ and $W'A'AW$) are in the middle of them around 1675 cm^{-1} , though they are unclear in the total spectrum. The peak at 1642 cm^{-1} arises mainly from $H'A'WA$ and $H'A'WAW$, and partly from $WAWW$, in which the CO bond accepts two HB donors. It is notable that the peak position correlates with the HB interaction energy of the CO bond. For example, the peak position lowers in the order of $W'A'AW$, WAW , and $WAWW$, (1673 , 1665 , and 1641 cm^{-1} ,

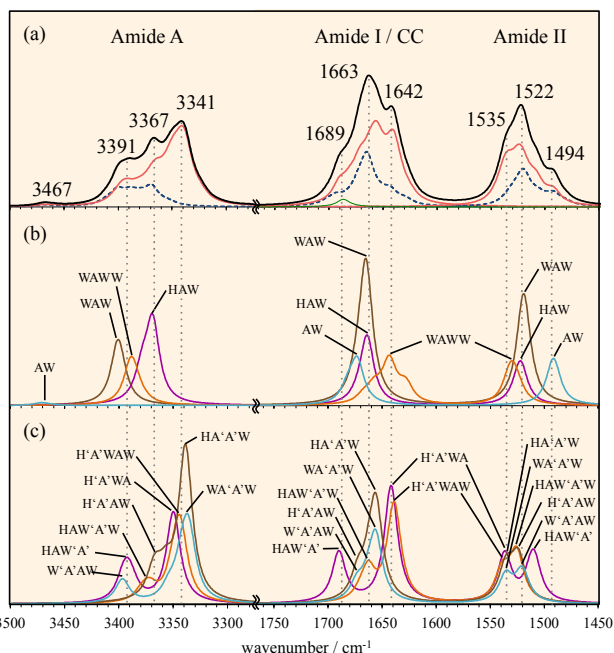
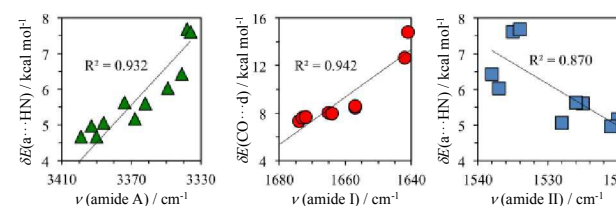


Fig. 8 Calculated IR spectrum of the amide I, II, A, and CC stretching modes of a SM bilayer in the gel phase. (a) The total spectrum (black), the amide bands of monomer and dimer of the amide group (blue and red, respectively), and the CC stretching band (green). (b) The amide bands decomposed in terms of major types of monomers. (c) The same as (b) but for dimers. The label of the amide group to which the mode is assigned is indicated with quotations as 'A'.

Table 5. The HB interaction energy^a of SM clusters (in kcal mol⁻¹).

type	a...d ^b	δE	a...d ^b	δE	a...d ^b	δE
WA	W...A	3.96				
AW	A...W	7.33				
WAW	W...AW	4.67	WA...W	8.04		
HAW	H...AW	5.17	HA...W	7.98		
WAWW	W...AWW	5.06	WA...2W	14.81		
WAAW	W...AAW	4.97	WA...AW	7.61	WAA...W	8.47
HAAW	H...AAW	5.60	HA...AW	7.68	HAA...W	8.50
HAWA	H...AWA	6.03	HA...WA ^c	12.65	HAW...A	4.67
HAWAW	H...AWAW	6.43	HA...WAW ^c	13.62	HAW...AW	5.63

^a $\delta E(X...Y) = E(X) + E(Y) - E(XY)$. ^b acceptor ... donor. ^c $\delta E(X...Y,Y) = E(X) + E(Y) + E(Y) - E(XYY)$.

**Fig. 9** Plots of the HB interaction energy with respect to the amide frequencies.

respectively), while the HB interaction energy increase as WA...AW, WA...W, and WA...2W (7.61, 8.04, and 14.81 kcal mol⁻¹, respectively). This behavior may be understood if we consider that the stronger HB makes the CO bond softer and shifts the CO stretching frequency lower. Plots of the HB interaction energy with respect to the peak position, displayed in Fig. 9, show surprisingly good linear correlation with $R^2 = 0.942$ manifesting the so-called Badger-Bauer rule.⁷⁴ Therefore, the fine structural peaks are caused by the HB motifs of different strength in a SM bilayer and the red-shift of the dimer band indicates that the stronger HBs grow dominant in the longer amide chain. The HB motifs may be the physical origin of the band components found in the experimental spectrum.⁷³

The amide A band reinforces the above argument that the spectral feature is dictated by the HB strength. The NH bond free of HB (AW) gives the leftmost, small peak at 3467 cm⁻¹. The NH bond donating to a water (WAW, WAWW, and W'A'AW) or to an amide group with a water (HAW'A' and HAW'A'W) gives the first intense peak at 3391 cm⁻¹, followed by the NH bond donating to a hydroxyl group (HAW and H'A'AW) at 3367 cm⁻¹. The rightmost peak at 3341 cm⁻¹ arises from H'A'WA, H'A'WAW, WA'A'W and HA'A'W, which give the strongest HB interaction energies among the NH donating pairs in Table 5. These peak positions correlate well with the HB interaction energy with $R^2 = 0.932$, as shown in Fig. 9.

The amide II band accompanies three peaks. The peaks at 1494 and 1522 cm⁻¹ are assigned to the NH bond free from HB and to the NH bond donating to a water or a hydroxyl group (e.g., WAW, HAW), respectively. The leftmost peak at 1535 cm⁻¹ is assigned to the NH bond with the strongest HB interaction (WA'A'W, HA'A'W, etc.). Thus, the blue-shift correlates with the HB interaction energy. The tendency may be understood that the stronger attractive force between the NH bond and

the HB acceptor makes the CNH bending vibration stiffer and thus shifts the frequency higher. The correlation between the peak positions and the HB interaction energy is also good with $R^2 = 0.870$.

The amide II and A bands have been observed in the IR experiment¹⁷ at 1553 and 3283 cm⁻¹, respectively, indicating that the calculated band positions are deviated by 30 - 50 cm⁻¹. One of the sources of error may be the treatment of anharmonicity. In this study, the harmonic frequency of SM clusters has been scaled by the factor derived from an isolated SM molecule. However, the factor may vary with respect to the strength of HB; most likely, the formation of strong HB would enhance the anharmonic effects. Note that the amide A band needs more red-shift, while the amide II band needs more blue-shift. The lack of the frequency shift in the opposite direction indicates that the anharmonic effects induced by HB need a more sophisticated treatment.

4 Conclusions

A new method is proposed to compute the vibrational spectrum of a SM bilayer combining the all-atom MD simulation with the vibrational structure calculation. In the proposed method, the classical trajectory obtained from MD is first analysed to detect clusters of SM and water molecules in a bilayer, followed by the vibrational structure calculation performed for each cluster based on DFT. Finally, the total vibrational spectrum is computed as the weight average of the spectrum of each cluster.

The Raman spectrum of a SM bilayer has been calculated for the amide I and the double bonded CC stretching modes. The calculated spectrum is in excellent agreement with the experiment, revealing the character of the band in question observed at 1643 cm⁻¹ to be the amide I vibration of SM clusters. The finding indicates that the amide I band serves as a marker to detect SM clusters in a bilayer. Therefore, Raman spectroscopy may open a new way to characterize the lipid rafts in biological membranes.

The IR spectrum is also calculated to be reasonably accurate compared to the experiment, although further effort is still needed to reproduce the band shape accurately. Nevertheless, the decomposition of the spectrum in terms of SM clusters has revealed that the band shape is primarily dictated by the strength of HB manifesting the Badger-Bauer rule. The calculated band positions of amide A and II modes are deviated by 30 - 50 cm⁻¹ compared to available experimental data due to an insufficient treatment of anharmonic effects.

A number of extensions of the present method are possible and undergoing; vibrational structure calculations with an explicit account of anharmonicity and dynamics, the use of QM/MM to treat the coupling with the environment, and so on. These developments in an aim to enhance the accuracy of prediction will be the scope of future studies.

Acknowledgements

This research is partially supported by “Molecular Systems” and “Integrated Lipidology” projects in RIKEN, the Center of innovation Program from Japan Science and Technology Agency, JST. K.Y. acknowledges financial support from Incentive Research Projects, RIKEN. We used computational resources provided by the HPCI System Research Project (Project ID: hp140105, hp150022, hp150023), the RIKEN Integrated Cluster of Clusters (RICC), and MEXT SPIRE Supercomputational Life Science (SCLS).

Notes and references

1. K. Simons and E. Ikonen, *Nature*, 1997, **387**, 569-572.
2. K. Jacobson, E. D. Sheets and R. Simson, *Science*, 1995, **268**, 1441-1442.
3. D. Lingwood and K. Simons, *Science*, 2010, **327**, 46-50.
4. M. T. Hyvönen and P. T. Kovanen, *J. Phys. Chem. B*, 2003, **107**, 9102-9108.
5. E. Mombelli, R. Morris, W. Taylor and F. Fraternali, *Biophys. J.*, 2003, **84**, 1507-1517.
6. R. M. Venable, A. J. Sodt, B. Rogaski, H. Rui, E. Hatcher, A. D. MacKerell, Jr., R. W. Pastor and J. B. Klauda, *Biophys. J.*, 2014, **107**, 134-145.
7. R. N. A. H. Lewis and R. N. McElhaney, *Chem. Phys. Lipids*, 1998, **96**, 9-21.
8. V. V. Volkov, D. J. Palmer and R. Righini, *Phys. Rev. Lett.*, 2007, **99**, 078302.
9. V. V. Volkov, D. J. Palmer and R. Righini, *J. Phys. Chem. B*, 2007, **111**, 1377-1383.
10. W. Zhao, D. E. Moilanen, E. E. Fenn and M. D. Fayer, *J. Am. Chem. Soc.*, 2008, **130**, 13927-13937.
11. M. D. Fayer, *Acc. Chem. Res.*, 2012, **45**, 3-14.
12. S. Nihonyanagi, J. A. Mondal, S. Yamaguchi and T. Tahara, *Annu. Rev. Phys. Chem.*, 2013, **64**, 579-603.
13. Y. Nojima and K. Iwata, *Chem. Asian J.*, 2011, **6**, 1817-1824.
14. Y. Nojima and K. Iwata, *J. Phys. Chem. B*, 2014, **118**, 8631-8641.
15. R. Faiman, *Chem. Phys. Lipids*, 1979, **23**, 77-84.
16. I. W. Levin, T. E. Thompson, Y. Barenholz and C. Huang, *Biochemistry*, 1985, **24**, 6282-6286.
17. O. P. Lamba, D. Borchman, S. K. Sinha, S. Lal, M. C. Yappert and M. F. Lou, *J. Mol. Struct.*, 1991, **248**, 1-24.
18. K. Shirota, K. Yagi, T. Inaba, P.-C. Li, Y. Sugita and T. Kobayashi, unpublished work.
19. P. R. Maulik and G. G. Shipley, *Biophys. J.*, 1996, **70**, 2256-2265.
20. P. R. Maulik and G. G. Shipley, *Biochemistry*, 1996, **35**, 8025-8034.
21. C. Yuan, J. Furlong, P. Burgos and L. J. Johnston, *Biophys. J.*, 2002, **82**, 2526-2535.
22. T. Terashima, M. Shiga and S. Okazaki, *J. Chem. Phys.*, 2001, **114**, 5663-5673.
23. M. Schmitz and P. Tavan, *J. Chem. Phys.*, 2004, **121**, 12233-12246.
24. M. Schmitz and P. Tavan, *J. Chem. Phys.*, 2004, **121**, 12247-12258.
25. R. D. Gorbunov, P. H. Nguyen, M. Kobus and G. Stock, *J. Chem. Phys.*, 2007, **126**, 054509.
26. B. M. Auer and J. L. Skinner, *J. Chem. Phys.*, 2008, **128**, 224511.
27. S. M. Gruenbaum and J. L. Skinner, *J. Chem. Phys.*, 2011, **135**, 075101.
28. S. M. Gruenbaum, P. A. Pieniazek and J. L. Skinner, *J. Chem. Phys.*, 2011, **135**, 164506.
29. S. M. Gruenbaum and J. L. Skinner, *J. Chem. Phys.*, 2013, **139**, 175103.
30. B. Auer, R. Kumar, J. R. Schmidt and J. L. Skinner, *Proc. Natl. Acad. Sci. U.S.A.*, 2007, **104**, 14215-14220.
31. Y.-S. Lin, B. M. Auer and J. L. Skinner, *J. Chem. Phys.*, 2009, **131**, 144511.
32. Y.-S. Lin, J. M. Shorb, P. Mukherjee, M. T. Zanni and J. L. Skinner, *J. Phys. Chem. B*, 2009, **113**, 592-602.
33. M. Cho, *J. Chem. Phys.*, 2003, **118**, 3480.
34. R. D. Gorbunov, D. S. Kosov and G. Stock, *J. Chem. Phys.*, 2005, **122**, 224904.
35. W. Zhuang, T. Hayashi and S. Mukamel, *Angew. Chem. Int. Ed.*, 2009, **48**, 3750-3781.
36. T. L. C. Jansen, A. G. Dijkstra, T. M. Watson, J. D. Hirst and J. Knoester, *J. Chem. Phys.*, 2006, **125**, 044312.
37. A. S. Bondarenko and T. L. C. Jansen, *J. Chem. Phys.*, 2015, **142**, 212437.
38. E. Malolepsza and J. E. Straub, *J. Phys. Chem. B*, 2014, **118**, 7848-7855.
39. H. Torii and M. Tasumi, *J. Raman. Spect.*, 1998, **29**, 81-86.
40. M. Nonella, G. Mathias and P. Tavan, *J. Phys. Chem. A*, 2003, **107**, 8638-8647.
41. B. Rieff, S. Bauer, G. Mathias and P. Tavan, *J. Chem. Phys. B*, 2011, **115**, 2117-2123.
42. M. Nonella, G. Mathias, M. Eichinger and P. Tavan, *J. Phys. Chem. B*, 2003, **107**, 316-322.
43. G. Babitzki, G. Mathias and P. Tavan, *J. Phys. Chem. B*, 2009, **113**, 10496-10508.
44. B. Rieff, S. Bauer, G. Mathias and P. Tavan, *J. Phys. Chem. B*, 2011, **115**, 11239-11253.
45. J. C. Phillips, et al., *J. Comput. Chem.*, 2005, **26**, 1781-1802.
46. W. L. Jorgensen, J. Chandrasekhar, J. D. Madura, R. W. Impey and M. L. Klein, *J. Chem. Phys.*, 1983, **79**, 926-935.
47. S. Jo, T. Kim, V. G. Iyer and W. Im, *J. Comput. Chem.*, 2008, **29**, 1859-1865.
48. J.-P. Ryckaert, G. Cicciotti and H. J. C. Berendsen, *J. Comp. Phys.*, 1977, **23**, 327-341.
49. T. Darden, D. York and L. Pedersen, *J. Chem. Phys.*, 1993, **98**, 10089-10092.
50. U. Essmann, L. Perera, M. L. Berkowitz, T. Darden, H. Lee and L. G. Pedersen, *J. Chem. Phys.*, 1995, **103**, 8577-8593.
51. S. Nosé, *J. Chem. Phys.*, 1984, **81**, 511-519.
52. W. G. Hoover, *Phys. Rev. A*, 1985, **31**, 1695-1697.
53. S. E. Feller, Y. Zhang, R. W. Pastor and B. R. Brooks, *J. Chem. Phys.*, 1995, **103**, 4613-4621.
54. W. Humphrey, A. Dalke and K. Schulten, *J. Mol. Graph.*, 1996, **14**, 33-38.
55. M. J. Frisch, et al., Gaussian 09 Revision D.01).
56. J. MacQueen, *Some methods for classification and analysis of multivariate observations*, University of California Press, Berkeley, California, 1967.
57. M. Feig, J. Karanicolas and C. L. Brooks, III., *J. Mol. Graphics Modell.*, 2004, **22**, 377-395.
58. A. D. Becke, *J. Chem. Phys.*, 1993, **98**, 5648-5652.

59. C. Lee, W. Yang and R. G. Parr, *Phys. Rev. B*, 1988, **37**, 785-789.
60. W. J. Hehre, R. Ditchfield and J. A. Pople, *J. Chem. Phys.*, 1972, **56**, 2257-2261.
61. P. C. Hariharan and J. A. Pople, *Theor. Chim. Acta*, 1973, **28**, 213-222.
62. T. Clark, J. Chandrasekhar, G. W. Spitznagel and P. V. R. Schleyer, *J. Comput. Chem.*, 1983, **4**, 294-301.
63. K. Yagi, S. Hirata and K. Hirao, *J. Chem. Phys.*, 2007, **127**, 034111.
64. K. Yagi, K. Hirao, T. Taketsugu, M. W. Schmidt and M. S. Gordon, *J. Chem. Phys.*, 2004, **121**, 1383-1389.
65. K. Yagi and H. Otaki, SINDO 3.6, RIKEN 2014.
66. K. R. S. Chandrakumar, T. K. Ghanty and S. K. Ghosh, *J. Chem. Phys.*, 2004, **120**, 6487-6494.
67. T. Mehnert, K. Jacob, R. Bittman and K. Beyer, *Biophys. J.*, 2006, **90**, 939-946.
68. C. Møller and M. S. Plesset, *Phys. Rev.*, 1934, **46**, 618-622.
69. R. A. Kendall, T. H. Dunning, Jr. and R. J. Harrison, *J. Chem. Phys.*, 1992, **96**, 6796-6806.
70. K. A. Peterson, D. E. Woon and T. H. Dunning, Jr., *J. Chem. Phys.*, 1994, **100**, 7410-7415.
71. H. Iikura, T. Tsuneda, T. Yanai and K. Hirao, *J. Chem. Phys.*, 2001, **115**, 3540-3544.
72. M. P. Veiga, J. L. R. Arrondo, F. M. Gofii, A. Alonso and D. Marsh, *Biochemistry*, 2001, **40**, 2614-2622.
73. Z. Arsov and L. Quaroni, *Biochim. Biophys. Acta*, 2008, **1778**, 880-889.
74. R. M. Badger and S. H. Bauer, *J. Chem. Phys.*, 1937, **5**, 839-851.